Temporary clogging effects induced by a sustainable anti-icing hydrogel on the hydraulic conductivity and inertia coefficient of open-graded asphalt pavements

Temporary clogging effects induced by a sustainable anti-icing hydrogel on the hydraulic conductivity and inertia coefficient of open-graded asphalt pavements

F. Autelitano[1a], D. Petrolo[a], L. Chiapponi[a], F. Giuliani[a], S. Longo[a]

[a]*Department of Engineering and Architecture, University of Parma, Parco Area delle Scienze 181/A, 43124 Parma, Italy*

Abstract

Open-graded asphalt pavements require special winter maintenance procedures to ensure the effectiveness of anti-icing and deicing measures. A recently developed solution for this type of pavement is represented by an environmental friendly thickened bio-based salt hydrogel, which consists of a thermo-sensitive sodium chloride (NaCl) brine admixed with a gellant agent (seaweed fibers) having the ability to form a gel-like structure when hot-sprayed on a cold surface. This thin salt layer results in a long-lasting residual efficacy of the winter maintenance product and in a reduction of salt consumption, but affects the drainage capacity of the pavement. These transient clogging effects were evaluated on laboratory-made specimens through the measurement of their vertical hydraulic conductivity variations before and after the hydrogel application, using a 1-D air permeameter and a constant head water permeameter. The analyses, based on Darcy-Forchheimer model and Darcy model for lower Reynold numbers, revealed a significant short-term reduction of the hydraulic conductivity, that, anyway, tends to be almost totally restored once the critical weather event is over (after about 6 hours).

Keywords: Winter maintenance, Porous asphalt, Permeable friction course, Highway, Hydraulic conductivity, Drainage capacity, Permeameter, Green solution

1. Introduction

Highway road agencies across the world have established the strategic goals of technological development and improvement of safety and comfort standards for users, making transportation enhancement an asset to the community. In this perspective, advanced pavement maintenance and rehabilitation represent two key elements to ensure the functional efficiency of the road network. As part of high-speed facilities' maintenance programs, the gradual replacement of end-of-life or damaged pavements with open-graded (permeable or porous) asphalt mixtures has been a strategy adopted to improve wet

[1]Corresponding author: federico.autelitano@unipr.it

weather driving conditions, upgrade the storm water management and mitigate the tire-pavement noise pollution [1, 2].

This process has meant that in some countries, e.g. Italy, the Netherlands and Japan, about 90% of the national highways are covered by open-graded asphalt pavements (OGAPs) [3, 4]. They are pavements in which the surface layer consists of an open-graded asphalt mixture, in which intermediate sized and fine aggregate fractions are omitted from the grading, with a very high ($> 16-18\%$) interconnected void content [5]. OGAP structure is generally composed by a multiple (1 to 4) open-graded layer system placed over an impervious concrete or dense-graded asphalt base. The rainwater drains vertically through the surface to the underlying layer and then it is laterally discharged. OGAPs have begun to be used since the early 1970s in several countries under a wide range of names, but following different constructive and design trajectories: porous asphalt (PA) and open-graded friction course (OGFC), also called permeable friction course (PFC), are the two most common definitions and types [6, 7]. Some original durability and maintenance issues have been overcome in the past decade thanks to changes in the mix-design, including (i) the increase of the target air void content, (ii) the use of higher quality binder (polymer modified asphalt or asphalt rubber) and (iii) the possible introduction of fibers and additives, which led to the development of new generation open-graded mixtures [8, 9].

Regardless of the construction technique, the benefits in terms of safety and environment of using OGAPs are manifold. These kind of pavements can minimize hydroplaning potential by improving the wet pavement frictional resistance and reduce water splash and spray as well as nighttime surface glare in moistened conditions, resulting in a significant reduction of road accidents and improvements in safety for the traveling public [10, 11]. Besides, the quick and direct infiltration of storm water helps to re-establish a more natural hydrologic balance, reduce runoff volume minimizing its negative consequences and improve the water quality, limiting the concentration of some pollutants either physically, chemically or biologically [12, 13]. Moreover, OGAPs are configured as quiet pavements, since they offer a systematic reduction of noise associated with the roadway operations [14].

Most of these inherent advantages of OGAPs depend on their drainage capacity, which is generally expressed in terms of hydraulic conductivity or surface infiltration rate. Although these terms are often used interchangeably, they do not represent the same quantity [15]. Specifically, hydraulic conductivity K, often indirectly defined by the intrinsic permeability coefficient κ, describes the efficiency of a porous medium to transmit fluid under a given hydraulic gradient; whereas the infiltration rate expresses the rate of volume flux of liquid flowing into the pavement per unit of surface area [16]. Thus, the hydraulic conductivity is a function of the dynamic viscosity of the fluid, of its specific weight and of the intrinsic permeability which, in turn, depends on the effective pore network of the mixture. Specifically, it is not only dependent on the total air voids, V_m, but also on other characteristics such as size distribution, shape, degree of connectivity and tortuosity of the pores [17, 18]. Besides the conventional laboratory procedures, based on the measurement of mixture densities and its volumetric properties, for determining the V_m, the water-accessible V_m, the voids filled with binder (VFB) and voids in the mineral aggregate (VMA) contents, several advanced methodologies were developed to in-depth analyze the internal void structure of asphalt mixtures. On the one hand, imaging techniques (e.g. X-ray computed tomography, nuclear magnetic

resonance) were used to non-destructively scan and reveal the 3-D internal details of real asphalt specimens [19, 20]. On the other hand, computational methods (e.g., discrete elements methods and intersected stacked air voids methods, statistical reconstruction, mathematical algorithms) were implemented to virtually reproduce, starting from mix-design data, the pore network model for dynamic simulations [21]. Considering permeable pavements in their most general meaning, including also pervious concrete, paving stones or interlocking concrete pavers, different methods have been implemented to directly assess their drainage capacity, such as single-ring and double-ring infiltrometers and permeameters [22, 23]. However, falling head and constant head permeameters are the most widely used devices for measuring the in situ drainability of an open-graded asphalt surfacing as well as for determining the vertical and horizontal hydraulic conductivity of cylindrical specimens of asphalt mixtures with interconnecting voids (cored out of the road or laboratory-made specimens) [24]. Some of these procedures are internationally codified (e.g. ASTM C1701, EN 12697:19, EN 12697:40), while others (e.g., ANAS, several DOT, LCS, etc.) represent internal standards to transportation agencies and road management authorities [6, 15, 25].

In addition of being an essential requirement at the design stage, a suitable surface hydraulic conductivity must also be maintained during the pavement service life. Pavement drainage potential can be significantly reduced over time by the clogging of the pores [16, 26]. The clogging process can primarily occur due to the deposition and retention of fine sediments and solid particles in the pavement pores. These debris, which are carried by wind or water (rainwater runoff) and transported by vehicles to the road surface, are mainly related to transport non-exhaust particle matters produced from the wearing down of brakes, tires and pavements, as well as the inorganic and organic matters derived from the surrounding environment (sand, silt, clay, dust) and overhanging vegetation [27, 28]. In cold environments, clogging is generally amplified by winter maintenance operations, mainly due to the passage of snowploughs and the spreading of solid deicers and/or abrasives (sand particles and rock chips) [14]. Some studies have observed that clogging usually affect only the surface or the upper layer of OGAPs, while others found that this phenomenon also occurs within the pavement structure or in the bottom layers [29]. When the drainage capacity of a porous pavement is significantly reduced, maintenance operations, including broom cleaning, vacuuming and high pressure jet washing, become necessary to restore a suitable hydraulic conductivity [30]. These interventions, in addition to be expensive and cause of traffic disruptions, could bring potential micro-damages to the pavement structure.

Besides clogging issues, some countries have experienced durability and maintenance problems with OGAPs in cold or freeze-thaw environments, which caused their discontinued use by several European road administrations (e.g. Germany, France, Belgium, Scandinavian regions) [31]. The open-graded layout makes these pavements more prone to short- and long-term raveling and more susceptible to the accelerated oxidative aging of the asphalt binder film coating the aggregates, leading to a reduced service life and a higher possibility of premature failures or damages [32, 5]. In parallel, the pavement structure rich of interconnected voids also influences the thermodynamic behavior of the pavement, which turns out to be more temperature sensitive [33]. Field measurements have shown that the surface of this kind of pavements in wintertime tends to be on average 2–4 °C degrees lower than a dense-graded. As a result, ice problems are likely to develop sooner (earlier and more frequent occurrence of black ice and hoarfrost/rime)

and last longer (longer time to recover the bare pavement) [34]. Thus, OGAPs require special winter maintenance procedures to ensure the effectiveness of anti-icing and deicing measures, which very often imply a greater salt consumption (up to 50%) or the use of alternative technologies and/or products to the traditional spreading of granular rock or marine salt (NaCl), liquid chloride-based brines (NaCl, $CaCl_2$ or $MgCl_2$) and possibly abrasives which tend to be trapped into the pore spaces (leaving the surface susceptible to icing and favoring clogging) or quickly drain through the pavement [35, 36, 37]. In this respect, the best anti-icing solution for OGAPs seems to be the use of more viscous and stickier agents to ensure a long-lasting residual effectiveness. Pre-wetted salt (dry NaCl + $CaCl_2$ brine) is generally used as soon as the porous pavement begins to freeze [38, 39]. But, new organic chemicals, mainly derived from the fermentation and processing of agricultural feedstock or cheese and beer brewing and known in the literature as agricultural-derived agro-based or ag-based products, characterized by enhanced properties are being developed and tested [40, 41]. Each agro-based compound, applied alone or diluted in deicer formulations, has a specific functionality. Thus, the addition of an organic thickening agent to a liquid brine can increase its viscosity, assuring a slower penetration and resulting in a reduction in bond strength between ice and pavement surface [42].

In this perspective, a recent study [43] has proposed to use a particular type of thickener, i.e. a phyto-based gellant, to formulate an enhanced NaCl brine for anti-icing interventions on OGAPs. Specifically, the potential of the wall-cell polysaccharides contained in seaweed fibers were exploited to prepare a liquid product, that hot-sprayed on a cold pavement surface has the ability to form a gel-like structure, making this anti-icing product able to temporarily fill the surface voids without permeating through the mixture. This behavior ensures a longer residual deicing effectiveness (certainly not less than that of a conventional brine prepared using the same salt concentration) without affecting the surface frictional properties of the pavement. On the basis of this recent technological advance, the same authors aim in this paper to analyze in details how the development of a temporary gel thin film on a OGAP affects its short-term (few hours) and long-term (at the end of the critical weather event) drainage capacity. These provisional clogging effects were evaluated on laboratory-made specimens of porous asphalt mixtures through the measurement of their vertical hydraulic conductivity variations before and after the hydrogel application. An original assessment of the air hydraulic conductivity was added to the traditional determination of the water one.

The paper is structured as follows. The theoretical approach to the problem is discussed in terms of similarity rules in §2. Materials and methods, including the description of the experimental facility, are presented in §3, while the test schedule and results are analyzed and discussed in §4. The conclusions are given in §5.

2. The filtration process in Darcy and in Forchheimer regime and similarity rules

Similarity rules analysis for filtration processes in the Darcy regime has already been applied in [24] and is now extended to the Forchheimer regime. Since, during the present experiments, the Reynolds number was often above the critical value where the inertial contributions become significant, this extension is required to assess if the calculated

similarity rules for the comparison between air and water are still valid throughout the range.

The phenomenon of the filtration process in a porous medium can be described by the following typical equation:

$$f(\Delta H, L, \rho, g, D, u, \mu, n, l_m) = 0, \tag{1}$$

where the variables are the scale of the diameter of the meati D, the characteristic path length L, the porosity n, related to the characteristics of the porous medium itself; the other variables are the fluid density ρ, the scale velocity u, the dynamic viscosity μ, which refer to the characteristics of the fluid. Some additional variables also appear, as the head variation ΔH, the gravity acceleration g and the mean free path of the molecules l_m. All the variables, except n, are dimensional. By applying Buckingham's theorem [see, e.g. 44], the 9 variables can be reorganized into 6 dimensionless groups, obtaining the following typical equation:

$$\tilde{f}\left(\frac{\Delta H}{D}, \frac{L}{D}, \frac{u^2}{gD}, \frac{\rho D u}{\mu}, n, \frac{l_m}{D}\right) = 0, \tag{2}$$

where L/D is experimentally irrelevant if $L \gg D$, and where the other groups can be rearranged acquiring some classical meaning, with $J = -\mathrm{d}H/\mathrm{d}L$ representing the hydraulic grade line, defined as the variation in the total head per unit variation of the length path. We also can combine the other parameters to obtain the Reynolds number $Re = \rho D u/\mu$, which is the ratio between inertial to viscous forces, and the Froude number, $Fr = gD/u^2$, which represents the ratio between inertial to gravity forces. The parameter n is already non dimensional and $Kn = l_m/D$ is the Knudsen number. Therefore, eq. (1) can be written as:

$$J = \tilde{f}(Re, Fr, n, Kn). \tag{3}$$

The Knudsen number has negligible effects if $Kn \to 0$ and can be dismissed. It has been experimentally observed that in the laminar regime, with $Re < Re_c$ and where Re_c is a critical Reynolds number, the relevant dimensionless groups can be combined, giving:

$$\frac{\gamma J D}{\rho u^2} = \frac{\Phi(n)}{Re}, \tag{4}$$

where γ is the specific weight of the fluid and $\Phi(n)$ is a function that depend on n. The velocity u from eq. (4) can be isolated, obtaining the well known Darcy's law:

$$u = \frac{1}{\Phi(n)} \frac{\gamma D^2 J}{\mu} = KJ, \tag{5}$$

which states that the fluid darcian velocity is directly proportional to the hydraulic gradient J times the hydraulic conductivity K. Equation (5) can also be written as

$$u = \frac{\gamma \kappa}{\mu} J, \quad \kappa = \frac{D^2}{\Phi(n)}, \tag{6}$$

where κ with the dimension $[\kappa] = L^2$ is the intrinsic permeability of the porous medium.

If the darcian regime is not applicable due to $Re > Re_c$, inertial effects must be considered [45, 46], which are generally approximated by a drag force expressed through a form-drag (dimensionless) coefficient C_D intervening in the typical equation:

$$\tilde{f}\left(\frac{\Delta H}{D}, \frac{L}{D}, \frac{u^2}{gD}, \frac{\rho D u}{\mu}, n, \frac{l_m}{D}, C_D\right) = 0. \tag{7}$$

The experimental combination of the dimensionless groups is the Forchheimer's extension of Darcy's law

$$J = \frac{\mu}{\gamma\kappa}u + \frac{C_D}{g\sqrt{\kappa}}|u|u, \tag{8}$$

also expressed as

$$J = \frac{1}{K}u + \left(\frac{\gamma}{\mu K}\right)^{1/2}\frac{C_D}{g}|u|u \tag{9}$$

or

$$J = \frac{1}{K}u + \frac{\beta}{g}|u|u, \quad \beta = C_D\left(\frac{\gamma}{\mu K}\right)^{1/2}, \tag{10}$$

where β is named inertial factor.

If the aim is to find a relationship between the hydraulic conductivity adopting air and water as fluid, the method of direct analysis can be applied [47] to eq. (10) to estimate the ratios of the relevant variables, which yields:

$$\begin{cases} r_J = \dfrac{r_u}{r_K}, \\ \\ r_J = \dfrac{r_u^2}{\sqrt{r_\nu r_K}}, \end{cases} \tag{11}$$

where r_i the scale ratio for the quantity i and where we have assumed $r_g = r_{C_D} = 1$ and $r_\nu = r_\mu / r_\rho$. Since $K = \gamma\kappa/\mu$, it holds $r_K = r_\kappa / r_\nu$.

For a fixed geometry, i.e. the same specimens with the same porosity and intrinsic permeability, it results $r_\kappa = 1$; if the interest is in measuring the hydraulic conductivity of the open-graded asphalt to air or water, then $r_\rho = \rho_{\text{water}}/\rho_{\text{air}}$ and $r_\mu = \mu_{\text{water}}/\mu_{\text{air}}$ are known. Hence, $r_K = 1/r_\nu$ and since $r_\nu = \nu_{\text{water}}/\nu_{\text{air}} \approx 10^{-1}$, it results $r_K \approx 10 \longrightarrow K_{\text{water}} \approx 10 K_{\text{air}}$.

As a final step, it is left to estimate:

$$\begin{cases} r_u = \dfrac{r_\mu}{r_\rho} = r_\nu, \\ \\ r_J = r_u^2, \end{cases} \tag{12}$$

hence,

$$r_u \approx 10^{-1} \implies u_{\text{water}} \approx 10^{-1} u_{\text{air}}, \tag{13}$$

$$r_J \approx 10^{-2} \implies J_{\text{water}} \approx 10^{-2} J_{\text{air}}. \tag{14}$$

The Reynolds number assumes the same value if water and air flowing in the same specimen are used, since $Re = uD/\nu \rightarrow r_{Re} = r_u / r_\nu = 1$, hence the flow regime is also correctly reproduced for both fluids. We also derive that $r_\beta = 1$.

In summary, the similarity ratios in eq. (11) hold independently of the flow regime.

Sieve (mm)	14.00	12.50	8.00	4.00	2.00	0.50	0.25	0.075
Cumulative passing (%)	100	98	30	13	11	8	7	5

Table 1: Selected grading curve.

3. Materials and Methods

3.1. Specimen of open-graded asphalt mixture production

An open-graded hot mix asphalt mixture for porous asphalt pavements was produced using a 50/70 polymer-modified asphalt cement (4.8% binder content by mass of dry aggregates), adopting a gradation curve for a permeable asphalt surface course, with a nominal maximum aggregate size of 12.5 mm (Table 1). These specifications derived from a mix design procedure adopted by an Italian highway agency. Laboratory-made cylindrical specimens, with a diameter $D = 100$ mm and a nominal thickness $t = 60$ mm, were prepared using the SuperPave gyratory compactor (Pine Instrument Company). The choice of the specimen height derives from the compromise between the most common thicknesses of open-graded asphalt layers (4–5 cm) and those dictated by hydraulic requirements for a correct measurement of the vertical hydraulic conductivity.

Preheated aggregates and asphalt cement were mixed at 160–170°C and then compacted in a specimen mold applying a constant vertical pressure of 200 kPa while rotating it for 30 gyrations (rate: 30 rpm; tilt angle: 1.25°). After demolding, the specimens were stored on a flat surface at laboratory conditions (temperature $T = 22 \pm 2$°C; relative humidity $RH = 55\%$) for 2 days and then weighted and their dimensions measured with a digital caliper. A total of 40 specimens have been produced for the experimental plan. On the basis of theoretical maximum density, ρ_m, of the uncompacted mixtures (EN 12697-5) and the bulk density, ρ_{bsea}, of the extruded specimens (12697-6: sealed specimen procedure), the air voids content, V_m, of the compacted specimens was calculated according to EN 12697-8 standard.

3.2. Seaweed–sodium chloride hydrogel preparation

The phyto-based sodium chloride hydrogel was formulated by adding a small quantity (2% by weight of the solvent) of seaweed fibers, i.e. marine red algae "ogonori", to a conventional NaCl brine generally used in winter maintenance operations. These ingredients ratios have proven to be ideal for the preparation of a sprayable and elastic gel, which combines suitable performances and limited fiber additions [43]. The gellant, which does not affect the thermal properties of the solvent, makes the salt brine able to form an almost transparent (pale straw yellow color for 0.5 mm thick film) and thermo-reversible gel-like structure, following an hot activation (melting $>$ 80–85°C) and a subsequent cooling that sets off the sol–gel transition (gelling $<$ 50–55°C). During the gel formation process, the material viscosity, η, increases from about 3 to 48 mPa s over the 80–55°C temperature range, with a sudden and very significant growth below the gelation point ($\eta \approx 130$ mPa s at 45°C). The gelling agent was diluted in a 23.3% wt.NaCl brine, which was preheated and kept on the hot plate of a magnetic stirrer at 90 ± 5 °C. The solution was then stirred for 5 minutes at 1000 rpm in a sealed glass container.

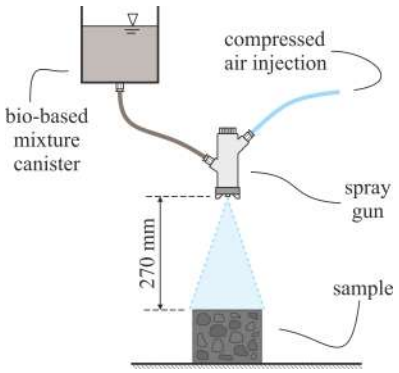

Figure 1: Schematic of the hydrogel spray system.

3.3. Hydrogel hot application

After having evaluated different saline gel application methodologies (spilling, spreading, spraying or pouring), the best performing solution for a thermo-sensitive material, which has the ability to form a gel by simply coming into contact with a very cold surface, resulted to be the air-atomized spraying of the hot liquid. This approach faithfully reproduces the product application on a road pavement during a winter maintenance operation. Thus, the phyto-based hydrogel was hot applied into liquid form (at $T = 70 \pm 5$ °C), using an air spray gun (figure 1), to the cold upper surface of the open-graded HMA specimens, which were preliminarily conditioned in a climatic chamber at 2.5 ± 0.5 °C for 12 h. Close to zero temperatures ($2 - 3$ °C) generally represent the first critical thermal threshold for the activation of predefined warnings and alarms in anti-icing management plans. A second subset of specimens instead underwent a water conditioning, i.e. soaking in a water bath inside a climatic chamber at 2.5 ± 0.5 °C for 48 h, to assess the possible influence of a moist surface on the gel application and adhesion. The spraying device consists of an applicator which atomizes the hydrogel by combining compressed air with liquid flow to form a pressurized mist. The amount of hydrogel being applied can be varied as a function of spraying time (pull-release of the trigger), distance of the spray tip from the surface and air pressure. Thus, the system was customized to achieve a homogeneous coverage and an even surface finish, applying a nominal quantity of hydrogel, q_n, equal to about 400 g/m^2. The spray gun was held at 27 cm to the target, keeping the spray fan at 90°. A specific air cup and nozzle were selected, as well as pattern and fluid control knob were adjusted, to obtain the desired spray pattern shape and film thickness. Moreover, an electro-mechanical valve was connected to the regulator of the air hose to automatically control the spraying time: after a series of trials in the described configuration, the duration of compressed air inflow was set to 0.8 s. Before every use, the canister was filled with hot water ($T = 75 \pm 5$ °C) and the valve was opened to continuously heat the hydraulic connections and the components inside the system, in order to avoid the subsequent gelification of the blend into the tubes and the nozzle.

Although the spraying procedure was almost automated, the amount of product which was spread on the specimens showed significant differences. Thus, each specimen was re-weighted to assess the actual applied material and this quantity (q_a) became an anal-

ysis parameter. Specimens were then divided in two subsets, which underwent different thermal treatments, i.e. storage at laboratory ($T = 20 \pm 2$ °C; $RH = 35 \pm 5\%$) and low temperature ($T = 2 \pm 0,5$ °C; $RH = 25 \pm 3\%$) conditions.

3.4. Hydraulic conductivity measurements

The effects of the hydrogel application on the hydraulic conductivity of porous asphalt pavements were evaluated though the measurement of the hydraulic conductivity variations to two different fluids, (i) water and (ii) air. Thus, experiments were carried out using two different types of permeameters, (i) the one-dimensional (1-D) air permeameter, and (ii) the constant head permeameter. Since one of the related functions of the phyto-based hydrogel is to fully restore the pavement hydraulic conductivity once the critical event is over, its evaluation took place at different time intervals after the application of the product: 0 (5 min after hydrogel application), 2, 6 and 24 h. For each thermal storage, the specimens were further divided into four sub-classes, which define the gaps between the gel application and test execution. This approach made the procedure more rigorous (maintenance of uniform conditions): each specimen was only once tested at the selected time with both the permeameters sequentially, measuring the air hydraulic conductivity at first and the water one immediately after. Repeating the tests on specimens previously exposed to a water flow would have induced the hydrogel degradation and affected the next analyses with the air permeameter due to the possible presence of water droplet trapped in the pores. In this way, the most critical condition in the evaluation of clogging effects was considered, in which no perturbing causes (traffic or precipitation) can favor the gel removal or dissolution. No less than 10 specimens were identified for each temporal interval: 5 for both conditioning procedures. The determination of the hydraulic conductivity before the gel spraying on the whole specimens set allows to define the reference condition. Some selected specimens were reused after an high pressure washing (to remove the gel film) and drying. In this way it was possible to increase the number of specimens limiting the inter-specimen variability (it must be noted that only the specimens which after washing showed a hydraulic conductivity close to the reference one were considered suitable for the reuse).

3.5. 1-D air laboratory permeameter

The 1-D air permeameter, shown in figure 2*a*, is made of polyvinyl chloride (PVC) cylinder 1 m long, with an internal diameter $D = 100\,\text{mm}$, and it is a replica of the device used by [24]. Each specimen is placed at the lower end of the cylinder, and a neoprene sheet with a thin film of vacuum grease is also applied between the specimen and the inner surface of the permeameter in order to secure the sealing and avoid any air leakage. The top end of the permeameter is connected to a source of pressurized air with a motorized needle valve that can adjust the air inflow rate. The cylinder is long enough to let the air inflow expand and homogenize before infiltrating in the porous medium. The air inflow rate is measured by a microbridge mass airflow sensor (Honeywell AWM5000 Series), with a range $0 - 333\,\text{ml}\,\text{s}^{-1}$, a linearity error equal to $\pm 3\%$ of reading (RD) and a repeatability of $\pm 0.5\%$ RD, including hysteresis effects. The differential pressure is measured by a capacitive differential manometer (Ashcroft XLDP), with a range ± 62 Pa and accuracy 0.5% full scale (FS). One of the ports of the manometer is connected to the rigid cylinder by means of three radial intakes located a few centimetres above the

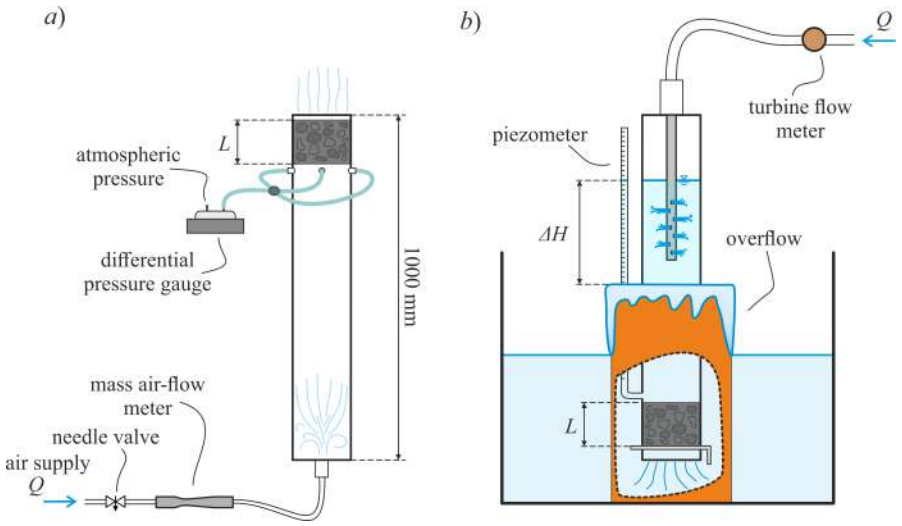

Figure 2: Experimental setup. *a*) 1-D air permeameter, and *b*) constant head permeameter for measurements with water.

specimen; the second port is open to the atmosphere. The manometer is calibrated before each experiment, by connecting it to a device that makes it possible to apply constant pressure measured by an inclined alcool column manometer. During the tests, the needle valve is progressively opened and closed twice, so the differential pressure and the air inflow rate are acquired for two completed cycles through a National Instruments Data Acquisition (DAQ) system at a data rate of 100 Hz. Figure 3*a* illustrates a typical example of two completed cycles, here shown for the specimen number 33. The pressure drop Δp is plotted versus the air inflow rate Q. Full symbols refer to the opening of the needle valve, while the empty symbols refer to the closure, while different colours refer to the first and second cycle. We can see that the behaviour of the specimen is homogeneous as the four branches of increasing and decreasing Q completely overlap and no hysteresis is observed. Figure 3*b* illustrates the behaviour of four different specimens, the specimens number 31, 33, 38 and 39. The modest difference between the four curves is due to the natural variability of the specimens, such as some small differences in compaction rate, void ratio or specimen geometry.

3.6. Constant head water permeameter

In order to measure the hydraulic conductivity of the porous asphalt to water, the constant head permeameter, sketched in figure 2*b*, was used. This permeameter is designed in accordance with the EN 12697-19 Standard and it consists of a cylindrical PVC pipe, with an internal diameter $D = 100$ mm, connected to a hydraulic bench with a pump and turbine flowmeter (OMEGA® FTB-4605), whit an accuracy equal to 1% RD. The specimen is at the downflow end of the pipe and held in place by a metallic rod. A piezometer is connected a few centimeters above the specimen in order to measure the upstream hydraulic head. Once the pump is switched on, water at a fixed inflow rate (60–250 ml s^{-1}) fills the permeameter and is forced to flow through the specimen. Water

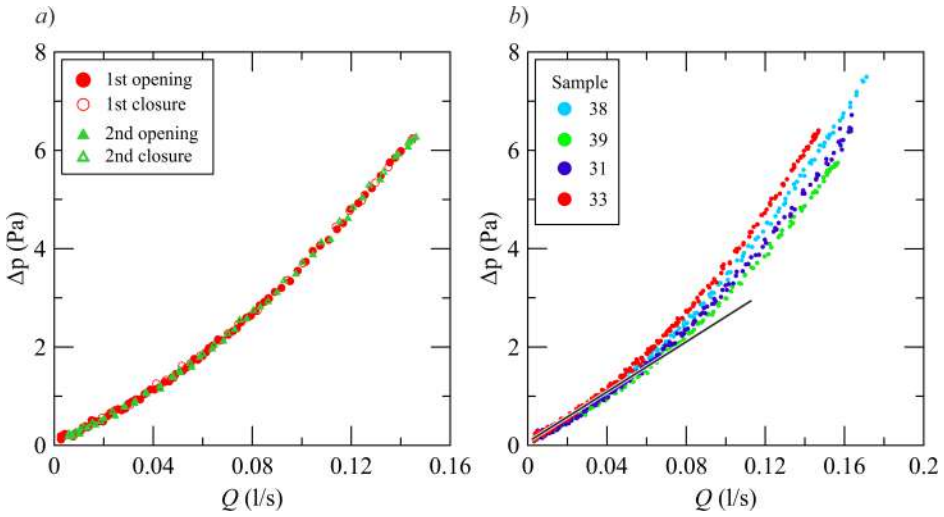

Figure 3: Pressure drop as a function of the inflow rate. *a*) Measurements with two cycles opening-closure for the specimen number 33, see table 2. Full symbols refer to the opening branch of the needle valve (waxing inflow rate), while the empty symbols refer to the closure branch (waning inflow rate); *b*) measurements for four different specimens, only waxing inflow rate. The line represents the Darcy approximation at low Reynolds number. Data are decimated for an easy visualization.

is then collected in an outer cylindrical pipe, with a larger diameter and closed bottom, which is placed around the permeameter to establish a constant downstream hydraulic head. In fact, when the outer cylinder is full of water, an overflows occurs at the top of it and the free surface level at that point represents the downstream head. The hydraulic head difference ΔH is kept constant through time thanks to a continuous supply of water from above. As the inflow rate is increased, a new equilibrium is reached by the system, with an higher water level in the piezometer, and hence in the upstream head. The excess water is collected in a big tank and repumped on top of the permeameter.

4. Results and analysis

The data analysis was articulated in two sequential sections. In a first step, the vertical hydraulic conductivity of the virgin untreated specimens was measured and studied, and subsequently the variation of this parameter after the application of the saline hydrogel was evaluated. A summary of the main dimensional, volumetric and hydraulic parameters of the prepared asphalt specimens is given in Table 2.

4.1. Air and water hydraulic conductivity of the untreated specimens

First of all, the experimental data in Table 2 report that the average ratio of hydraulic conductivity with water and with air is ≈ 6.1, in fairly good agreement with the theoretical predictions and with the deviations attributed to the lower accuracy of the estimates in water (4 or at most 5 measuring points, compared to a continuous measurement of several thousand values for air). However, the ratio of the β coefficients is about 0.1, whereas it should be unitary. Again, the origin of the discrepancy can be attributed

specimen	m (g)	h (cm)	$K_{\mathrm{Fh-air}}$ (cm s^{-1})	β_{air} (cm^{-1})	$K_{\mathrm{Fh-water}}$ (cm s^{-1})	β_{water} (cm^{-1})	κ_{air} (cm^2)	κ_{water} (cm^2)	Vm (%)
									-
1	803.13	6.30	0.66	823	3.1	81	1.16	0.83	-
2	804.83	6.25	0.54	943	3.5	100	1.43	1.02	-
3	799.54	6.03	0.50	1109	3.1	114	1.63	1.16	20.17
4	801.89	6.10	0.63	836	3.3	85	1.21	0.87	-
5	798.23	6.13	0.72	742	5.3	109	1.56	1.11	-
6	798.92	5.99	0.62	870	4.3	120	1.71	1.22	-
7	795.73	5.90	0.43	1357	5.0	250	3.57	2.55	-
8	800.78	6.03	0.49	1072	3.1	93	1.33	0.95	-
9	798.42	6.05	0.55	960	3.8	111	1.58	1.13	-
10	837.36	6.42	0.70	732	5.6	140	2.00	1.43	-
11	802.01	6.08	0.55	1002	3.4	100	1.43	1.02	-
12	806.25	6.02	0.60	896	3.5	117	1.67	1.19	-
13	802.54	6.04	0.62	838	5.4	121	1.73	1.23	-
14	792.86	5.90	0.46	1283	2.9	170	2.43	1.73	-
15	801.01	6.04	0.60	867	3.2	93	1.33	0.95	-
16	796.67	6.10	0.72	737	3.4	90	1.28	0.92	-
17	801.53	5.97	0.57	901	4.0	100	1.43	1.02	19.08
18	799.33	5.99	0.52	1006	3.0	85	1.21	0.87	-
19	796.93	6.00	0.55	920	3.3	110	1.57	1.12	-
20	803.87	6.10	0.48	975	3.2	115	1.64	1.17	-
21	802.86	6.05	0.54	884	3.6	105	1.50	1.07	-
22	800.41	6.10	0.48	1175	3.2	160	2.28	1.63	-
23	800.98	6.05	0.52	1023	3.3	125	1.78	1.27	-
24	801.13	6.05	0.53	1004	4.1	140	2.00	1.43	19.26
25	799.24	6.07	0.59	779	3.0	66	0.94	0.67	19.93
26	801.36	6.07	0.52	907	3.2	100	1.43	1.02	-
27	806.89	6.12	0.50	965	2.6	80	1.14	0.82	20.75
28	799.54	6.15	0.64	801	3.5	80	1.14	0.82	-
29	802.11	6.25	0.77	665	2.7	40	0.57	0.41	21.96
30	796.71	6.07	0.52	1073	4.2	140	2.00	1.43	-
31	809.33	6.15	0.56	888	2.8	90	1.28	0.92	-
32	803.54	6.13	0.53	873	2.7	69	0.99	0.70	20.02
33	799.91	6.06	0.50	1108	3.0	100	1.43	1.02	-
34	799.86	6.00	0.51	1024	3.9	140	2.00	1.43	-
35	787.76	5.86	0.31	1881	3.5	270	3.85	2.75	-
36	799.58	6.04	0.54	1020	3.2	130	1.86	1.33	20.01
37	806.82	6.01	0.63	912	2.6	100	1.43	1.02	19.52
38	806.17	6.14	0.54	1005	2.2	40	0.57	0.41	-
39	810.83	6.16	0.60	869	3.2	104	1.48	1.06	19.90
40	804.17	6.03	0.48	1100	2.2	70	1.00	0.71	-
mean $\pm$std		6.1 ± 0.1	0.56 ± 0.09	970 ± 210	3.4 ± 0.8	110 ± 45	1.6 ± 0.6	1.1 ± 0.4	20.1 ± 0.8

Table 2: List of the specimens and parameters. m is the mass of the specimen, h is the height, $K_{\mathrm{Fh-air/water}}$ and $\beta_{\mathrm{air/water}}$ are the estimated hydraulic conductivity and inertial factor for air and water, respectively, according to Darcy-Forchheimer model, $\kappa_{\mathrm{air/water}}$ is the intrinsic permeability estimated in experiments with air/water, Vm is the void ratio. The uncertainty refers to 1 std.

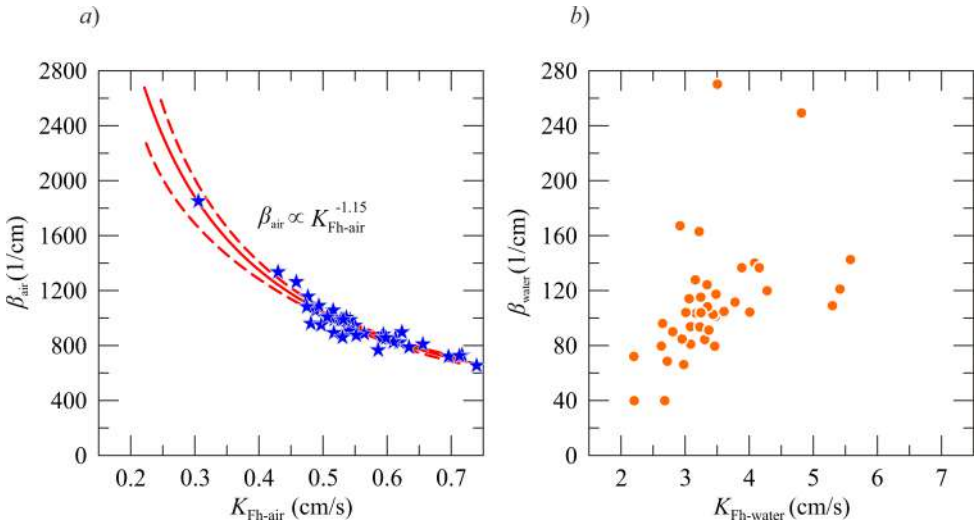

Figure 4: Correlation between β and K_{Fh} *a*) for air, and *b*) for water. Symbols refer to experimental data, the bold curve refers to the interpolating power function, dashed curves refer to 95% confidence limits.

to the accuracy of the measurement procedure, which is much higher for air than for water. Figure 4*a*-*b* shows the value of the inertial factor as a function of the hydraulic conductivity, evaluated according to the Forchheimer model, for all the specimens listed in Table 2 and for air and water, respectively. The dependence $\beta_{\mathrm{air}} - K_{\mathrm{Fh\text{-}air}}$ in figure 4*a*, appears particularly consistent, in agreement with the conceptual scheme and with numerous empirical-semiempirical relationships reported in the literature. For instance, [48, 49] for measurements in limestone, dolomite and sandstone specimens, calculated $\beta \propto \kappa^{-5/8} n^{-3/4}$, where κ is the intrinsic permeability and n is porosity; the value of the exponent is different also from theory, where $\beta \propto \kappa^{-05}$, but one must bear in mind the different nature of the specimens with β affected to some extent by pore structure, see also [50]. The same dependence for water in figure 4*b*, however, appears much less consistent. It is also noted that the intrinsic permeability κ calculated on the basis of the estimates with air and with water does not assume a single value, being in average $\approx 50\%$ greater for air than for water. The authors hypothesize that this discrepancy may be caused by some air bubbles that, during the flow with water, remain attached and block some interconnected voids. In addition, the limited number of points in the in-water measurements (4 or 5) significantly reduces the accuracy of the estimate.

4.2. Air and water hydraulic conductivity of the specimens after the phyto-based gel application

The visual inspection of specimens' surface over time offers a reading key of the gel-structure evolution after being sprayed. Figure 5*a*-*b* display a photo of the upper face of a specimen before and after the hydrogel application. Specifically, figure 5*b* highlights how the gel, which has a glossy finish, tends to fill the surface voids, leaving the aggregates almost exposed and the specimen's macro-texture recognizable. The change of the gel film appearance over time (2, 6, and 24 h after the spray) in both storage

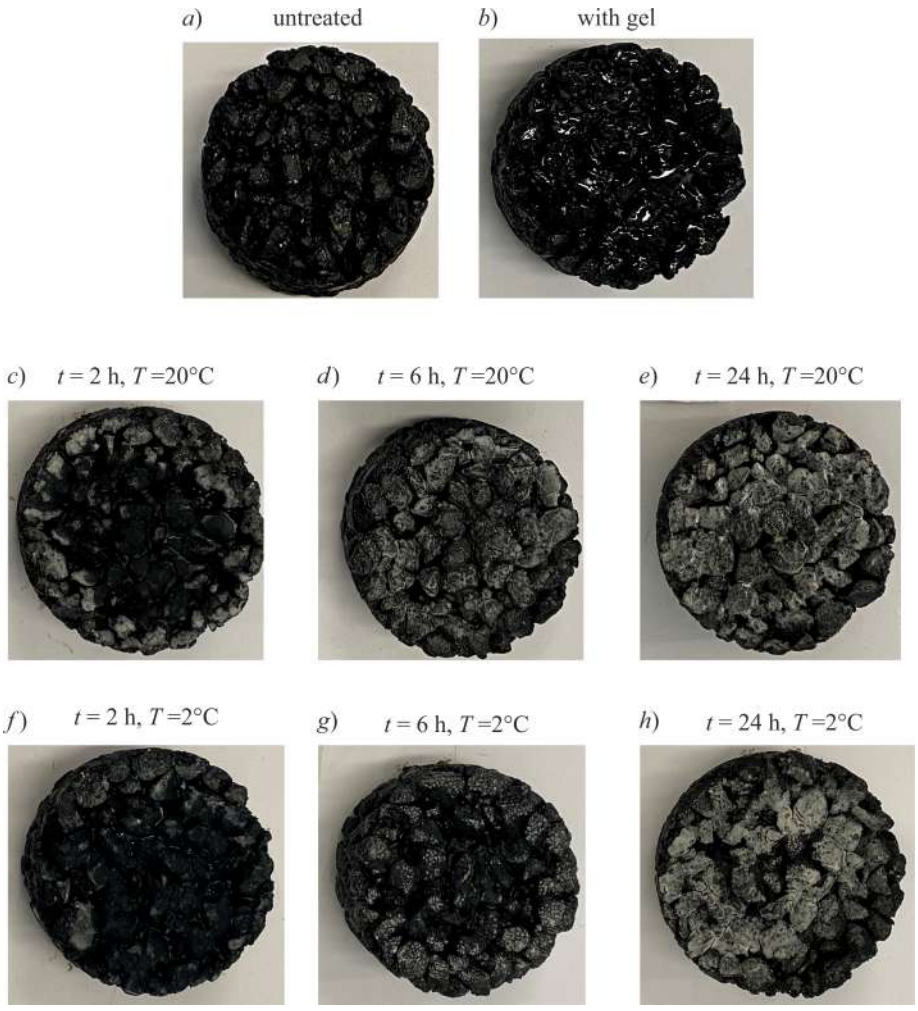

Figure 5: Photographs of the upper face of some specimens. *a*) Untreated specimen; *b*) specimens immediately after gel application; *c*)-*d*)-*e*) specimens stored at $T = 20°\mathrm{C}$ after $2 - 6 - 24$ h after the spray of the gel; *f*)-*g*)-*h*) specimens stored at $T = 2°\mathrm{C}$ after $2 - 6 - 24$ h.

conditions is depicted in figure 5*c-d-e* ($T = 20°C$) and figure 5*f-g-h* ($T = 2°C$). The salt blend does not permeate at higher depths, but rather stays in place on the surface, due to the gel-like structure that forms immediately after the spray because of the high temperature gradient. Generally speaking, the hydrogel applied on specimens stored at ambient temperature undergoes a rather quick drying and shrinkage, so the liquid part evaporates while the solid part, typically the salt and the insoluble fibers, remain on the surface. This behavior is less noticeable and occurs more slowly at lower temperatures.

The measurements performed with air are very suitable for an interpretation according to the Forchheimer model $J = au + bu^2$, with several measurements performed continuously and with an adequate accuracy of the instruments. For this reason, the comparison between the specimens before treatment and after gel treatment was performed for the hydraulic conductivity k_{Fh}, equal to the inverse of the coefficient a, and for the inertial factor β equal to bg, where g is the acceleration of gravity. Figure 6 shows the variation in the air hydraulic conductivity $\Delta K_{\mathrm{Fh-air}}$ as function of the amount of mixture sprayed on the specimens, q. As expected, the reduction in the air hydraulic conductivity increases with q, without a specific trend for specimens stored at room temperature and in the fridge. Data show a significant dispersion, but can be interpolated by the equation $\Delta K = 0.058q - 2 \cdot 10^{-4}q^2$ (ΔK in percent and q in g/m^2), and the minimum quantity to gain a 20% reduction is 500 g/m^2. Figure 7 shows the variation of the inertial factor β_{air} as function of q. We observe that, apart from a few specimens, the inertia coefficient grows with q, with two distinct trends for the short-term and long-term specimens. This means that the set-up of the porous medium after the spray evolves in a relevant way: at first, the gel waterproofs only the most superficial layers, with a reduction of hydraulic conductivity due almost exclusively to the upper layers, while the airflow in the lower layers is not significantly modified; subsequently, it seems that the gel, eventually fragmented, modifies the hydraulic conductivity throughout the thickness of the specimen, with an increase of β that more closely responds to the theoretical model, i.e. β inversely proportional to K. This behaviour is even more evident in figure 8, where the variation of β with K is shown.

The analysis of the variation of hydraulic conductivity for water was conducted in a different way. In fact, the number of measurement points for water is generally 4, which is too small to allow accurate estimations by the Darcy-Forchheimer model. For this reason, the comparison of the hydraulic conductivity of water before and after treatment was carried out using the linear Darcy approximation. Figure 9 shows the variation in the water hydraulic conductivity $\Delta K_{\mathrm{water}}$ as function of the amount of mixture sprayed on the specimens, q. The trend of decreasing hydraulic conductivity for the specimens after treatment is also evident for water. The dependence of permeability on time is varied. Immediately after spraying, the gel is compact and, in sufficiently large quantities, significantly reduces permeability; as time elapses, the gel tends to fragment and peel off, reducing its effectiveness. For sufficiently long times, however, the fragments eventually tend to occlude the pores, with recovery of effectiveness comparable to that immediately post-spraying. The effect of storage temperature of the specimens, on the other hand, appears less obvious and sharp, and does not allow for clear interpretation.

4.3. The time dependence of hydraulic conductivity in treated specimens

As described in sections 3.3 and 3.4, the hydrogel was sprayed on the upper surface of the specimens, which were immediately weighed to actually calculate how much product

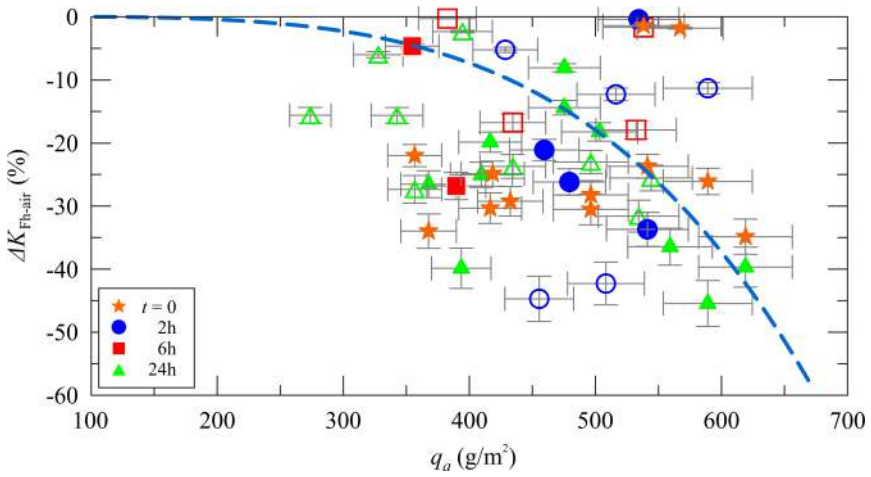

Figure 6: Variation of the hydraulic conductivity as a function of the quantity of the bio-based hydrogel, for experiments with air, immediately after spraying the bio-based compound, after 2 h, 6 h, and 24 h. Bold symbols refer to specimens stored in the fridge ($T = 2 \pm 0.5\,^{\circ}\text{C}$, $RH = 25 \pm 3\%$), empty symbols refer to specimens stored in air ($T = 20 \pm 2\,^{\circ}\text{C}$, $RH = 35 \pm 5\%$). Error bars refer to 1 std.

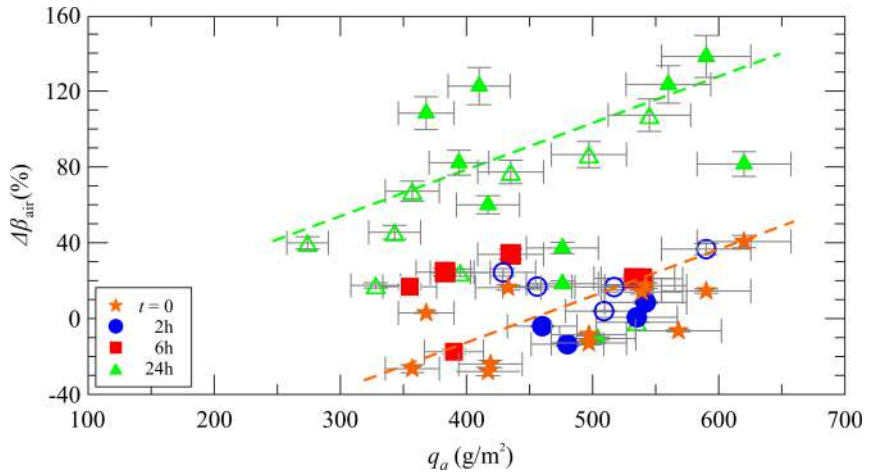

Figure 7: Variation of the inertial factor for experiments with air. For caption, see figure 6. The dashed lines are the linear interpolating curves for the early time (orange stars) and the 24 h (green triangles) specimens.

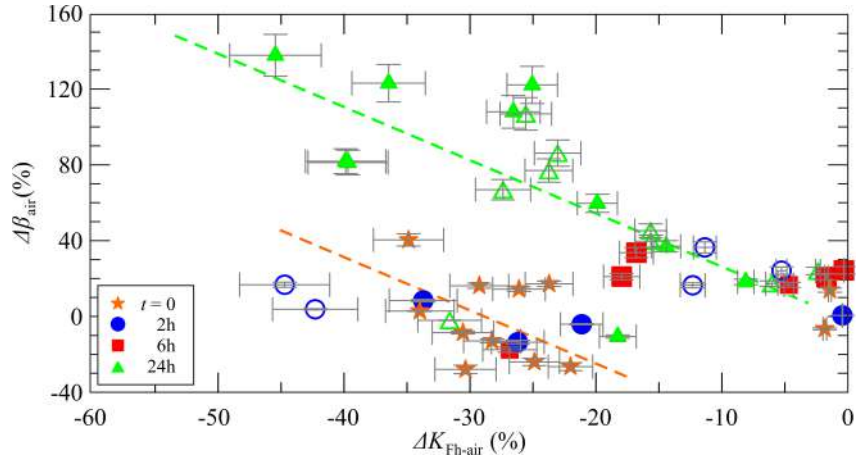

Figure 8: Variation of the inertial factor as a function of the hydraulic conductivity, for experiments with air. For caption, see figure 6. The dashed lines are the linear interpolating curves for the early time (orange stars) and the 24 h (green triangles) specimens.

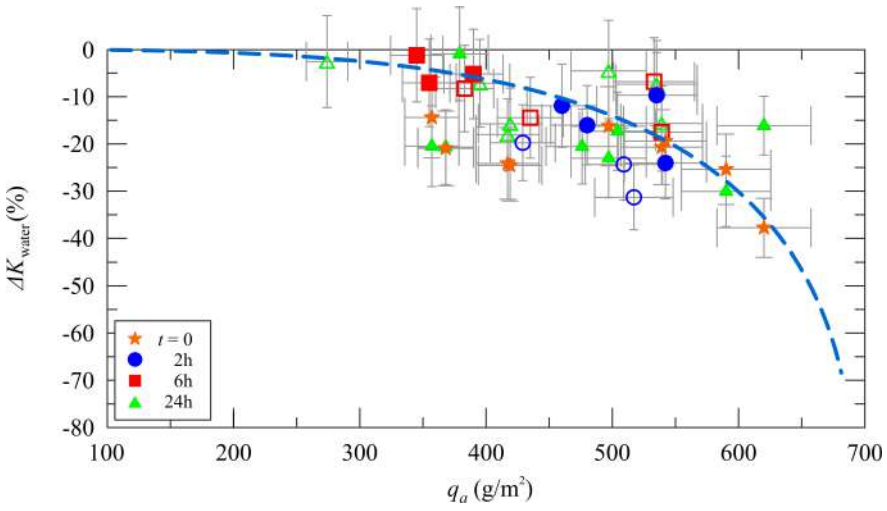

Figure 9: Variation of the hydraulic conductivity as a function of the quantity of the bio-based hydrogel, for experiments with water, immediately after spraying the bio-based compound, after 2 h, 6 h, and 24 h. Bold symbols refer to specimens stored in the fridge, empty symbols refer to specimens stored in air. Error bars refer to 1 std.

had been applied (q_a). The specimens of the 0-time class were immediately subjected to the air hydraulic conductivity test, followed by the water hydraulic conductivity test. An initial comparison was made on the percentage reduction of the parameters ΔK_{air} and ΔK_{water} after spraying, depending on the amount of mixture applied to the specimen. The results are shown in figure 10*a-b*. It is emphasized that the quantity q_a describes, in all graphical representations, the amount of gel effectively spread on specimens' surface immediately after spraying. With the exception of two outlayers, in the case of air hydraulic conductivity the trend is in the direction of decreasing hydraulic conductivity as the amount of applied product increases, as expected. The two points deviating from the trend line could be due to the fact that the mixture was not evenly distributed over the specimen. As far as the hydraulic conductivity to water is concerned, the experimental points that are referred to as outlayers in figure 10*a* align well with the other values in the graph. In this case, no well-defined trend line can be seen, but there is a more or less constant reduction in hydraulic conductivity of 20% up to quantities of product reaching 500 g/m^2, after which, for larger quantities of product, there is a further reduction in hydraulic conductivity.

The 2h-class refers to specimens which were stored for 2 h after hydrogel application. After 2 hours, these specimens were weighed again to check the amount of gel lost during storage, and the hydraulic conductivity to air and water was then calculated. Specimens stored in a fridge show a weight loss of $6 \pm 2\%$ compared to the calculated post-spray weight, while those left in an airy environment have a reduction in the order of 20%. Figure 10*c-d* shows the hydraulic conductivity variation for this subset of measurements. With the exception of one outlayer point, where a low amount of mixture was applied, an average reduction of 20% in both water and air hydraulic conductivity was measured in all other specimens. The values of K_{air} and K_{water} were slightly higher than those measured immediately after the application of the product.

After 6 hours in the air and in the fridge, the watery part of the mixture has evaporated to a large extent and salt residues can be seen; in the voids, however, part of the product remains, which in both cases is still soft and firm. The weight reduction in this case is in the order of 35% in both storage configurations. Figure 10*e-f* shows the hydraulic conductivity variation for this further subset of measurements. In this case, a minimal reduction in hydraulic conductivity, of the order of 10% in water and 5% in air, was observed; in some cases an increase in hydraulic conductivity is measured, but these are outlayers. It can therefore be concluded that the hydraulic conductivity after 6 hours is close to that of the original pavement.

To confirm the restoration of hydraulic conductivity, tests were carried out 24 hours after spraying. The weight loss compared to the time after spraying is 50% for specimens stored in the fridge and 70% for those stored in air. In both cases, a white patina remains on the surface due to the salt, some of the voids have cleared but some product is still present. Figure 10*g-h* shows the hydraulic conductivity variation for this third subset of measurements. hydraulic conductivity is almost completely restored, with only two cases showing a reduction in hydraulic conductivity to water of 20% in two specimens stored in a fridge, where the lack of a ventilated environment probably allowed the mixture to store better and a considerable amount of product is still present.

It can be concluded that the application of the mixture to the pavement results in a higher hydraulic conductivity reduction in the first few hours after treatment; once part of the mixture has dried, the hydraulic conductivity slowly returns to its original value,

but some salt remains on the pavement surface.

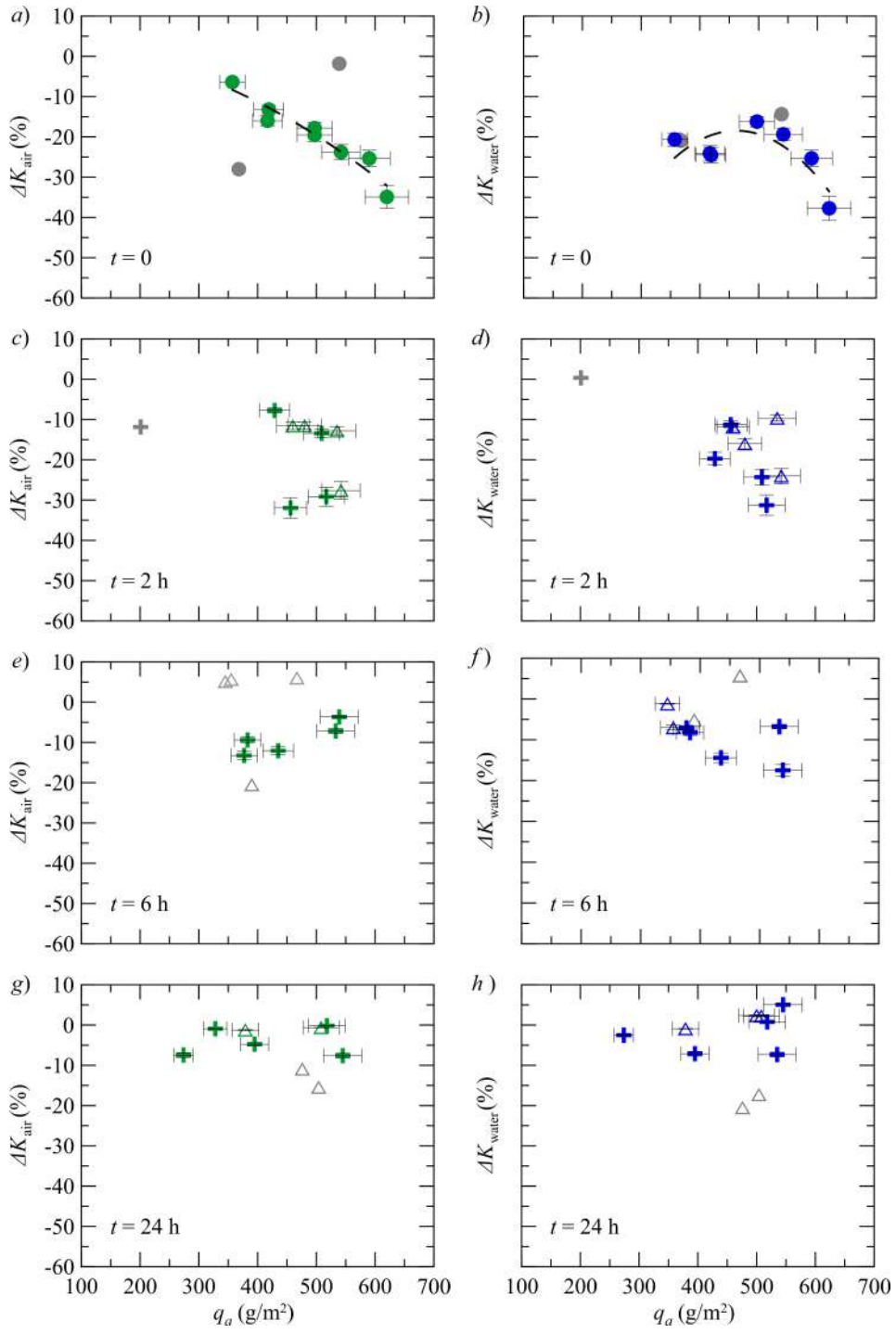

Figure 10: Variation of the hydraulic conductivity as a function of the time from treatment, for experiments with water and air, *a*)-*b*)immediately after spraying the bio-based compound, *c*)-*d*) after 2 h, *e*)-*f*) after 6 h, and *g*)-*h*) after 24 h. Bold symbols refer to specimens stored in the fridge, empty symbols refer to specimens stored in air, gray symbols are outalyers. Error bars refer to 1 std.

5. Conclusion

A promising newly conceived solution for winter maintenance interventions on open-graded asphalt pavement, based on the spraying of a thermo-sensitive salt hydrogel, highlights a temporary hydraulic conductivity reduction as side effect. The complete validation of this type of product can not ignore the assessment of the pavement pre- and post-treatment hydraulic conductivity. Two different methodological approaches had been adopted to perform these measurements. Specifically, an air permeameter was set up to avoid the possible effects of gel dilution due to water filtration and to perform a more rigorous testing, but a conventional water permeameter was also used for comparison, since beside to be a codified standard procedure it better reproduces the real conditions during a rain or storm event.

The filtration regime during the experiments was initially Darcian, at small inflow rate, and then became Forchheimer-like, with a two-parameter estimate, namely hydraulic conductivity K and the coefficient of inertia β. In the case of the air measurements, the two experimental parameters traced the theoretical inverse proportionality relationships with high accuracy; in the case of water, the correlations appeared inconsistent, presumably as a result of the limited number of experimental points for hydraulic conductivity estimated with water. For this reason, the variation of the parameters with the amount of gel sprayed and at increasing time since application was analyzed with reference to the Forchheimer model for air measurements, and with reference to hydraulic conductivity alone for tests with water.

As expected, hydraulic conductivity decreased for increasing amount of gel sprayed per unit area. But, this reduction resulted to be an extremely time-dependent process. The gel film quickly evolved after its application: the hydrogel underwent a drying and shrinkage induced by the evaporation of its liquid component.

This phenomenological description of the gel behavior was also reflected in the measured K values. After a significant reduction of hydraulic conductivity in both air and water (about 20–25% for 400 $\mathrm{g\,m^{-2}}$ gel) registered in the first hours after spraying, an evaluation of it after 6 h showed only small changes from the pre-treatment values of about 10%. After 24 h, the original hydraulic conductivity of the open-graded specimens was almost fully restored, testifying how the temporary clogging effect, which is a short-term requirement to prolong the product residual efficacy, exhausted in times comparable with those of critical weather events. The practical implications of these findings concern the actual possibility of exploiting the potential of a technology based on a bio-based salt hydrogel for structuring sustainable winter maintenance operations without adversely affecting the long-term characteristics of the open-graded asphalt pavements.

Funding

This research has financially been supported by the Program "FIL-Quota Incentivante 2019" of University of Parma and co-sponsored by Fondazione Cariparma.

References

[1] Z. Zhang, A. Sha, X. Liu, B. Luan, J. Gao, W. Jiang, F. Ma, State-of-the-art of porous asphalt pavement: Experience and considerations of mixture design, Construction and Building Materials 262 (2020) 119998.

[2] M. A. Hernandez-Saenz, S. Caro, E. Arámbula-Mercado, A. E. Martin, Mix design, performance and maintenance of Permeable Friction Courses (PFC) in the United States: State of the Art, Construction and Building Materials 111 (2016) 358–67.
[3] Direzione Generale per la Vigilanza sulle Concessionarie Autostradali, Relazione attività 2018, Technical Report, Ministero delle Infrastrutture e dei Trasporti, Roma, 2021.
[4] S. Takahashi, Comprehensive study on the porous asphalt effects on expressways in Japan: Based on field data analysis in the last decade, Road Materials and Pavement Design 14 (2013) 239–55.
[5] H. Wu, J. Yu, W. Song, J. Zou, Q. Song, L. Zhou, A critical state-of-the-art review of durability and functionality of open-graded friction course mixtures, Construction and Building Materials 237 (2020) 117759.
[6] Transportation Research Board and National Academies of Sciences Engineering and Medicine, Annotated Literature Review for NCHRP Report 640, The National Academies Press, Washington, DC, 2009.
[7] P. S. Kandhal, Design, construction, and maintenance of open-graded asphalt friction courses, National Asphalt Pavement Association: Lanham, MD, 2002.
[8] A. de Bondt, K. Plug, J. van de Water, P. The, J. Voskuilen, Development of a durable third generation porous asphalt with a high noise reduction, 6th Eurasphalt & Eurobitume Congress (2016).
[9] C. B. Nielsen, Durability of porous asphalt-international experiences, Danish Road Directorate, 2006.
[10] J.-S. Chen, C. H. Yang, Porous asphalt concrete: A review of design, construction, performance and maintenance, International Journal of Pavement Research and Technology 13 (2020) 601–12.
[11] R. Elvik, P. Greibe, Road safety effects of porous asphalt: a systematic review of evaluation studies, Accident Analysis & Prevention 37 (2005) 515–22.
[12] M. E. Barrett, Effects of a permeable friction course on highway runoff, Journal of Irrigation and Drainage Engineering 134 (2008) 646–51.
[13] J. Liu, M. Borst, Performances of metal concentrations from three permeable pavement infiltrates, Water Research 136 (2018) 41–53.
[14] D. C. Gibbs, R. Iwasaki, R. Bernhard, J. Bledsoe, D. Carlson, C. Corbisier, K. Fults, T. Hearne Jr, K. McMullen, D. Newcomb, et al., Quiet pavement systems in Europe, Technical Report, Federal Highway Administration, Washington, DC, 2005.
[15] C. Stanard, R. Candaele, R. J. Charbeneau, M. E. Barrett, State of the Practice Permeable Friction Courses, Technical Report, Texas Department of Transportation, Austin, TX, 2007.
[16] R. J. Charbeneau, J. B. Klenzendorf, M. E. Barrett, Methodology for determining laboratory and in situ hydraulic conductivity of asphalt permeable friction course, Journal of Hydraulic Engineering 137 (2011) 15–22.
[17] Y. Zhao, X. Wang, J. Jiang, L. Zhou, Characterization of interconnectivity, size distribution and uniformity of air voids in porous asphalt concrete using x-ray ct scanning images, Construction and Building Materials 213 (2019) 182–93.
[18] J. Chen, X. Yin, H. Wang, X. Ma, Y. Ding, G. Liao, Directional distribution of three-dimensional connected voids in porous asphalt mixture and flow simulation of permeability anisotropy, International Journal of Pavement Engineering 21 (2020) 1550–62.
[19] J. B. Król, R. Khan, A. C. Collop, The study of the effect of internal structure on permeability of porous asphalt, Road Materials and Pavement Design 19 (2018) 935–51.
[20] X. Ma, J. Jiang, Y. Zhao, H. Wang, Characterization of the interconnected pore and its relationship to the directional permeability of porous asphalt mixture, Construction and Building Materials 269 (2021) 121233.
[21] J. Zhu, T. Ma, Z. Lin, J. Xu, X. Qiu, Evaluation of internal pore structure of porous asphalt concrete based on laboratory testing and discrete-element modeling, Construction and Building Materials 273 (2021) 121754.
[22] V. C. Andrés-Valeri, M. Marchioni, L. A. Sañudo-Fontaneda, F. Giustozzi, G. Becciu, Laboratory assessment of the infiltration capacity reduction in clogged porous mixture surfaces, Sustainability 8 (2016) 751.
[23] H. Li, M. Kayhanian, J. T. Harvey, Comparative field permeability measurement of permeable pavements using ASTM C1701 and NCAT permeameter methods, Journal of Environmental Management 118 (2013) 144–52.
[24] F. Giuliani, D. Petrolo, L. Chiapponi, A. Zanini, S. Longo, Advancement in measuring the hydraulic conductivity of porous asphalt pavements, Construction and Building Materials 300 (2021) 124110.
[25] M. Kayhanian, H. Li, J. T. Harvey, X. Liang, Application of permeable pavements in highways for

stormwater runoff management and pollution prevention: California research experiences, International Journal of Transportation Science and Technology 8 (2019) 358–72.
[26] T. Fwa, E. Lim, K. Tan, Comparison of permeability and clogging characteristics of porous asphalt and pervious concrete pavement materials, Transportation Research Record 2511 (2015) 72–80.
[27] B. K. Ferguson, B. K. Ferguson, Porous pavements, Taylor & Francis: Boca Raton, FL, 2005.
[28] M. L. Afonso, C. S. Fael, M. Dinis-Almeida, Influence of clogging on the hydrologic performance of a double layer porous asphalt, International Journal of Pavement Engineering 21 (2020) 736–45.
[29] M. Z. H. Mahmud, N. A. Hassan, M. R. Hainin, C. R. Ismail, R. P. Jaya, M. N. M. Warid, H. Yaacob, N. Mashros, Characterisation of microstructural and sound absorption properties of porous asphalt subjected to progressive clogging, Construction and Building Materials 283 (2021) 122654.
[30] L. Liu, G. Yao, J. Zhang, S. Wu, Evaluation of effectiveness of cleaning on in situ permeability restoration of open-graded friction course, Journal of Transportation Engineering, Part B: Pavements 146 (2020) 04020003.
[31] Vejdirektoratet, Winter Service of Porous Asphalt. European Experience, Technical Report Technical note 123 – 2012, Copenhagen. Danish Road Directorate, Copenhagen, 2012.
[32] K. Zhang, J. Kevern, Review of porous asphalt pavements in cold regions: the state of practice and case study repository in design, construction, and maintenance, Journal of Infrastructure Preservation and Resilience 2 (2021) 1–17.
[33] J. Livet, J. Roussel, Comprendre le comportement hivernal des enrobés drainants, Technical Report, Laboratorie Central des Pontes et Chausses & Service d'Études des routes et Autoroutes, Paris & Bagneux, Paris & Bagneux, 1993.
[34] J. Livet, Evaluation des bétons bitumineux drainants en termes d'exploitation hivernale d'un réseau routier, Bulletin des Laboratoires des Ponts et Chaussées (1996) 15–23.
[35] M. Akin, L. Fay, X. Shi, Friction and snow–pavement bond after salting and plowing permeable friction surfaces, Transportation Research Record 2674 (2020) 794–805.
[36] F. Autelitano, M. Rinaldi, F. Giuliani, Winter highway maintenance strategies: Are all the sodium chloride salts the same?, Construction and Building Materials 226 (2019) 945–52.
[37] Y. Yildirim, T. Dossey, K. W. Fults, M. Trevino, Winter maintenance issues associated with new generation open-graded friction courses, Technical Report FHWA/TX-07/0-4834-1, Texas Department of Transportation, Austin, TX, 2006.
[38] World road association (PIARC), Snow and Ice Databook 2022. XVI World Winter Service and Road Resilience Congress, PIARC: La Défense, 2022.
[39] N. Takahashi, S. Tanaka, R. A. Tokunaga, F. Tayu, K. Takeichi, S. Kami, H. Sakakibara, Ice formation and the effectiveness of deicing agent on porous asphalt and stone mastic asphalt, Transportation Research Record 2482 (2015) 57–66.
[40] A. Muthumani, X. Shi, Effectiveness of liquid agricultural by-products and solid complex chlorides for snow and ice control, Journal of Cold Regions Engineering 31 (2017) 04016006.
[41] L. G. Terry, K. Conaway, J. Rebar, A. J. Graettinger, Alternative Deicers for Winter Road Maintenance - A Review, Water, Air, & Soil Pollution 231 (2020) 1–29.
[42] X. Shi, S. Jungwirth, The Search for "Greener" Materials for Winter Road Maintenance Operations, John Wiley & Sons: Hoboken, NJ, 2018.
[43] F. Autelitano, S. Longo, F. Giuliani, Phyto-based sodium chloride hydrogel for highway winter maintenance of porous asphalt pavements, Construction and Building Materials 319 (2022) 126082.
[44] S. Longo, Applications in Fluid Mechanics and Hydraulics, In *Principles and Applications of Dimensional Analysis and Similarity*, Springer International Publishing, Cham, 2021, pp. 177–218.
[45] D. A. Nield, A. Bejan, Convection in porous media, volume 3, Springer, 2006.
[46] A. Barletta, Routes to Absolute Instability in Porous Media, Springer, 2019.
[47] S. Longo, The Theory of Similarity and Applications to Models, In *Principles and Applications of Dimensional Analysis and Similarity*, Springer International Publishing, Cham, 2021, pp. 135–73.
[48] D. Cornell, D. L. Katz, Flow of gases through consolidated porous media, Industrial & Engineering Chemistry 45 (1953) 2145–52.
[49] J. D. Janicek, D. L. V. Katz, Applications of unsteady state gas flow calculations, in: University of Michigan (Ed.), Proceedings of Research Conference Flow of Natural Gas from Reservoirs, 1955.
[50] P. Macini, E. Mesini, R. Viola, Laboratory measurements of non-Darcy flow coefficients in natural and artificial unconsolidated porous media, Journal of Petroleum Science and Engineering 77 (2011) 365–74.